

FIG. 1. The setup and readout scheme for the trapped-ion quantum computer. (a) Schematic of our experimental setup. A single ion fluoresces inside an ion trap and its radiated photons are collected by a 0.37 NA lens. This fluorescence is then imaged onto a single channel of a multi-channel photo-multiplier tube detector. (b) Energy levels in the  $^{171}\text{Yb}^+$  atomic system used for fluorescence detection. If the qubit state is  $|0\rangle$ , the applied detection laser is off resonance and nearly no photons are scattered. If the state is  $|1\rangle$  the transition is on resonance and the ion fluoresces strongly.

tion time follows a near-Poissonian distribution, centered around 0 for state  $|0\rangle$  (the “dark” state) and 9 counts for state  $|1\rangle$  (the “bright” state) following a 150  $\mu\text{s}$  integration time. The deviations from Poissonian statistics indicate the error mechanisms in this readout scheme. The dark state histogram includes a small contribution at higher counts due to off-resonant dark-to-bright pumping during the detection step [26]. More importantly, the bright state histogram has a non-Poissonian tail towards lower photon counts due to off-resonant excitation to the  $|^2P_{1/2}, F=1\rangle$  manifold, detuned by 2.1 GHz, from which decay to  $|0\rangle$  is possible[26]. By choosing an optimal collection time, 150  $\mu\text{s}$  in our system, the overlap between the photon distributions corresponding to  $|0\rangle$ , and  $|1\rangle$  can be minimized. Thus, by discriminating the two distributions one can deduce the state of the qubit. One of the

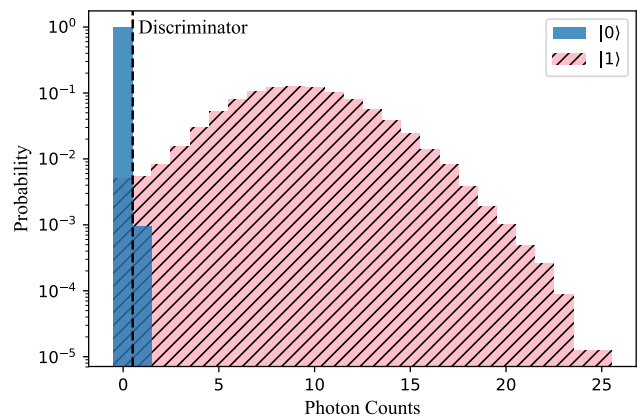


FIG. 2. The histogram of observed photons for an integration time of 150  $\mu\text{s}$  for state detection. The photon counts follow a Poisson distribution, in which the state  $|0\rangle$  (solid blue) gives a mean close to zero, while the state  $|1\rangle$  (shaded pink) results in nine photons on average.

commonly used techniques to distinguish between these distributions is a simple threshold discriminator, where instances with observed photon counts greater than the threshold are taken to be  $|1\rangle$ , and those below to be  $|0\rangle$  (see Fig. 2). This method works very well in the single qubit case and results in a detection fidelity, that is  $\mathcal{F} = p(\text{measured } x | \text{prepared } x)$ , of 99.4% for  $|1\rangle$ , and 99.6% for  $|0\rangle$ , which gives an average detection fidelity of 99.5% in our setup. This error can be reduced by increasing the collection angle of the objective and reducing the detection time. A readout fidelity of  $\sim 99.99\%$  has been demonstrated using this method [27].

Similar dark-to-bright or bright-to-dark pumping errors exist in other readout schemes, e.g., when a separate state with a finite lifetime is used as the dark state, known as a shelf state [7]. Smaller error contributions include laser light scattering off the ion trap and into the PMT as well as PMT dark counts, which account for 20 counts per second and 2 counts per second respectively. Both of these errors contribute only one false count for an average of 300 experiments and are therefore well discriminated using a thresholding method.

When detecting the state of more than one qubit, a bright ion can cause events on other ion detector channels. This crosstalk between the PMT channels modifies the distribution of observed photons, and the average detection fidelity decreases. One can choose a different threshold for each ion based on the state of its neighbors to partially mitigate these errors. In addition, using maximum likelihood methods, one can calculate the probability that an observed data point corresponds to the  $|0\rangle$  or  $|1\rangle$  state, and choose the most probable option [7, 28]. However, these methods are all tailored for a specific scenario and it is difficult to integrate other sources of information about the state, such as counts from extra PMT channels when imaging the ions onto alternating detectors, or photon arrival times. The latter

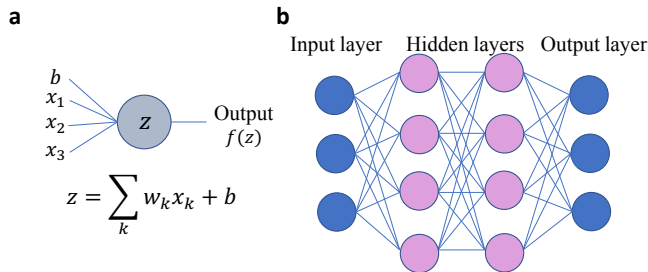


FIG. 3. An artificial neuron and a neural network. (a) A single neuron takes inputs  $x_k$  and outputs  $f(\sum_k w_k x_k + b)$ , where  $f$  is called the activation function, and  $w_k$ 's and  $b$  are weights and the bias of the neuron. (b) A neural network is composed of artificial neurons stacked in layers and connected to each other.

contributes information about the state because bright-to-dark or dark-to-bright pumping events have characteristic photon arrival time distributions, i.e. photons arriving predominantly early or late in the detection window, which can be included in the discrimination procedure. To incorporate all data sources in a single framework and reduce the effect of crosstalk we take advantage of advances in the field of machine learning, and use an artificial neural network to perform the discrimination task. Before proceeding to the main results, we briefly introduce the neural network framework that is used in this work.

With  $N$  qubits, the measurement consists of photon counts and their arrival times on  $M \geq N$  PMT channels. These photon counts can be binned into  $T$  time-bins to give  $M \times T$  numbers that completely describe the measurements. Our goal is to classify these measurement results into  $2^N$  states, in an  $N$ -qubit basis. Therefore, we consider a supervised learning scenario, where a set of measurement results and their corresponding state labels is used to train the machine and predict the correct state corresponding to a given input. We use a feed-forward neural network as depicted in Fig. 3 [29]. The network is built from a collection of neurons arranged in layers (columns in Fig. 3). A single neuron takes the inputs  $x_k$ , and outputs  $f(\sum_k w_k x_k + b)$ , where  $f$  is called the activation function, and  $w_k$  and  $b_k$  are weights and biases respectively. One example of activation functions is the rectifier  $f(z) = \max(0, z)$ . The first layer is called the input layer, where the neurons output the input data. Here, we have  $M \times T$  neurons representing integrated photon counts from each ion in a time-bin (pixel values in Fig. 4). The last layer of the network is called the output layer. For classifying data into exclusive classes, it is common to use a softmax activation at the output layer, i.e.  $f_j(z_1, z_2, \dots, z_k, \dots) = \frac{e^{z_j}}{\sum_k e^{z_k}}$ . This choice of activation normalizes the output and can be interpreted as the probability of each input data belonging to each class  $j$ , and the output with the highest probability is chosen as the label  $\hat{y}$ . These classes correspond to the

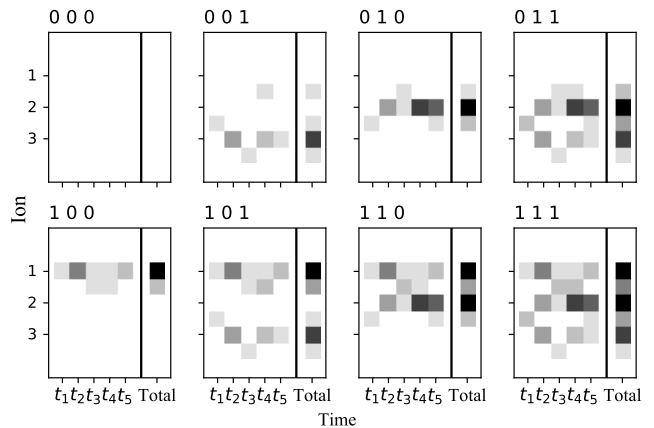


FIG. 4. Results of an instance of the experiment for different initial states. Photon counts for all eight computation basis states over three qubits (000,001,...,111) are binned into  $30 \mu\text{s}$  time-bins in a total of  $150 \mu\text{s}$  collection. The last column shows the total counts and darker color indicates more photons. The effect of crosstalk is visible in the intermediate channels (unlabeled rows).

$2^N$  different quantum states in our system (image labels in Fig 4). All the layers between the input and output are called hidden layers, and we use the rectifier function for them. We use a neural network with two hidden layers. The number of neurons in these layers varies from 8 for the simplest case to 40 for the network with the most features. The training task consists of finding weights and biases that optimize a cost function. We minimize the cross-entropy with the ADADELTA optimizer [30].

We now discuss the results in detail. We begin by moving a single trapped ion to the positions that would be occupied by ions in the multi-ion chain that we wish to investigate. This method allows us to recreate the experimental setup with  $N$  qubits. We typically image ions onto alternating PMT channels to reduce the crosstalk, which leaves the intermediate channels unused. We also take data imaging them onto neighboring PMT channels in order to explore how detection errors would change for a chain of ions with smaller inter-ion distance. Then, we either initialize the ion in  $|0\rangle$  to take data on dark states or we use a high-fidelity microwave pi-pulse to create  $|1\rangle$  for bright-state data. Finally, we detect the qubit state by counting how many photons are detected on the ion's corresponding PMT channel as well as neighboring channels. In addition, the photon arrival time is recorded with sub- $\mu\text{s}$  resolution. By loading only a single ion, we can create the full statistics for all the  $2^N$  computational basis states by superimposing these individual distributions. This procedure separates SPAM errors from other systematic errors present in the system such as addressing crosstalk errors. The average detection fidelity, which includes a small error from state preparation, is given by

$$\bar{F} = 1/\mathcal{N} \sum_i p(\text{measured } i | \text{prepared } i), \quad (1)$$

where the sum is carried over all the computational basis states.

We compare six different methods and show that machine learning approaches outperform the two commonly used strategies in state discrimination. In this comparison, we train the neural network on 80% of the data, and report the fidelities on the remaining 20% test set. Below we describe these six strategies:

- (i) Fixed threshold (*FT*): A threshold for photon counts is chosen to maximize the discrimination between bright and dark probability distributions. The same threshold is used for all the ions. In experiments with more than one qubit, this threshold is higher than the single qubit case because of crosstalk. Additional background noise from superimposing the statistic of individual qubits do not significantly contribute to errors.
- (ii) Adaptive threshold (*AT*): The threshold for each ion depends on the state of its neighbors. First, the state is determined by a fixed threshold, and then the inference process is iterated based on the state of neighbors and the corresponding thresholds.
- (iii) Neural network (*NN*): First the photon counts from the ion PMT channels and their corresponding  $2^N$  states (labels) are fed into a neural network. After the training, the neural network can predict the state of a given array of photon counts.
- (iv) Neural network with intermediate channels (*NN+*): Similar to *NN*, but the input also contains the intermediate PMT channel's data.
- (v) Neural network with time-stamped data (*TNN*): The photon counts from the ion PMT channels are collected into time-bins to form a 2D image, where one axis is the time, and the other represents the location of the ions. The color intensity then represents the number of photons observed in that time-bin (see Fig. 4). These images with their corresponding labels are used to train the neural network.
- (vi) Neural network with time-stamped data and intermediate channels (*TNN+*): The time-binned photon counts of the ion PMT channels and the intermediate channels are used to form an image, which the neural network learns to classify. This is the most comprehensive information available about the experiment.

We note that due to a large overlap between the photon count distributions of the intermediate channels with different bright neighbors, it is not possible to utilize the intermediate channel data with a simple threshold method. The same is true for the time-binned data, where the overlap of the bright and dark distributions is significant. This is because the distributions are Poissonian and have

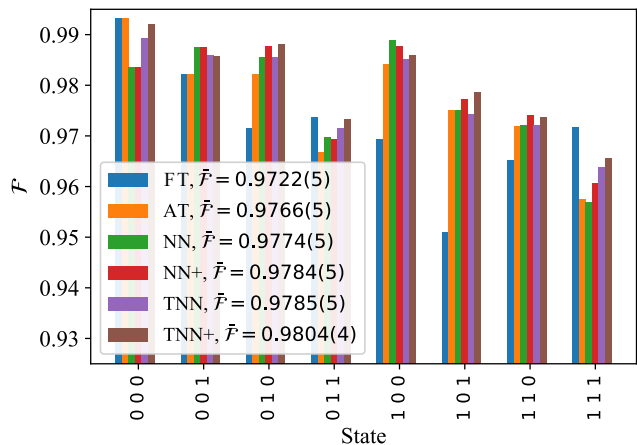


FIG. 5. Comparison of different methods for state detection defined in the main body. We can see that the neural network (*NN*) methods outperform the conventional thresholding (*FT*, *AT*) methods. In addition, the performance is enhanced gradually as we provide the neural network with more features, e.g. intermediate channels and time stamps. The errors given in parentheses are statistical.

close mean values. However, the neural network can easily incorporate all the features and extract the available information.

In the first experiment, we consider a three qubit measurement scenario where the data from intermediate channels is available. We collect 80000 samples for each label and apply the six strategies and observe that the neural network outperforms the other methods. In Fig. 5, it can be seen that with the same amount of information *NN* outperforms *T* and *AT*, and when additional information is provided *TNN+* can improve the errors over *T* and *AT* by 30% and 17% respectively. It can also be seen that the neural network reduces the false positives in detecting 000 and 111 states and improves the crosstalk errors in the other states. Note the architecture of the neural network is kept the same and only the number of neurons are increased to represent the more complicated features, therefore providing a flexible tool for inferring properties of the system from experimental data.

In the second experiment, the ions are moved closer to each other to represent experiments where there are many ions in the trap, and neighboring PMT channels are associated with different ions. In this case, the data from intermediate channels is no longer available, and the crosstalk errors are increased. We consider a five qubit measurement scenario with 50000 samples for each label and compare *T*, *AT*, *NN* and *TNN* methods.

As shown in Fig. 6 we can see that the same behavior observed in the first experiment persists, and neural networks beat threshold methods, and incorporating time stamped data further improves the fidelities. Specifically, we observe 29% and 6% improvement by *TNN* over *T* and *AT*, respectively.

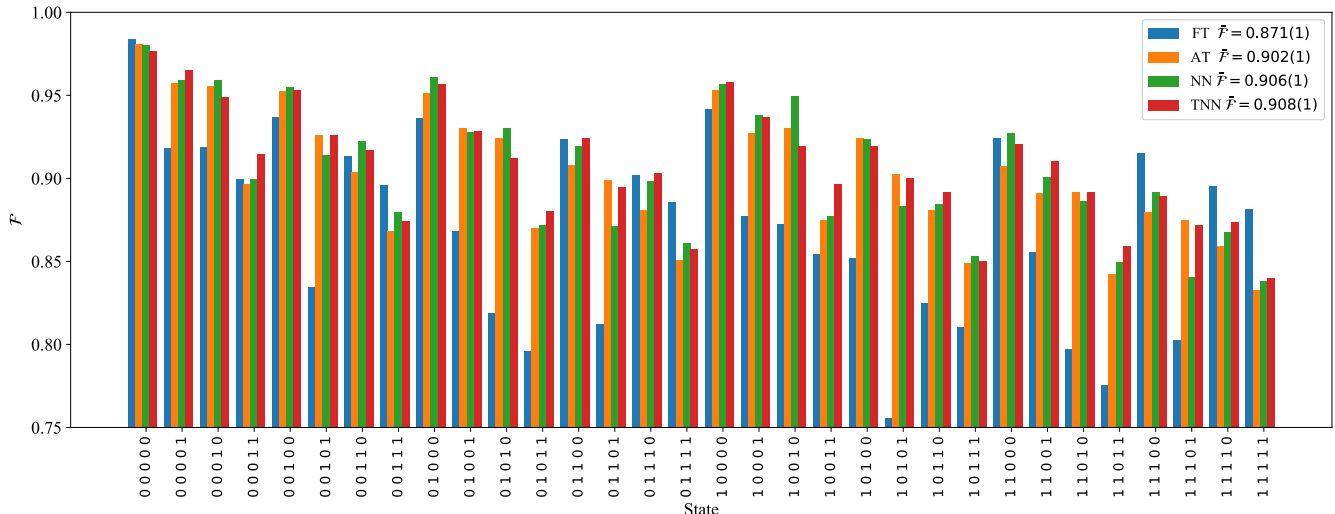


FIG. 6. Comparing neural networks with threshold methods for five-qubit state detection. In this case the intermediate channel data is not available, but neural networks can still perform better than threshold methods. The errors given in parentheses are statistical.

In addition, we employ a recurrent neural network (RNN) as an alternative approach. These networks are tailored towards studying sequences of data (time-bins in our case), where the output in each step depends on the history through the internal state and an external input (see Fig. 7 inset). This feedback and memory effect is useful in capturing correlations in the sequence. While we observe the same fidelity as  $TNN+$ , this method is advantageous for experiments with variable detection time, since it can handle data sequences with different lengths. We illustrate this capability by training a long short-term memory (LSTM) network, which is a type of RNN [31], with the full sequence of measurement data, using finer time-bins of  $10\mu s$ . Then, we evaluate the performance of the network by varying the length of the test sequence, and observe that indeed the performance increases with the measurement time (see circles in Fig. 7). In addition, we interrogate the network with artificial data to map out its internal mechanism. Specifically, we construct sequences with a single photon count, the arrival time of which is scanned. The output indicates the significance of the photon arrival time in deciding the state of the qubits. We observe that the network learns that photons with late arrival times are more likely to come from ions prepared in the dark state, which is consistent with our physical understanding of error mechanism by off-resonant excitation (see triangles in Fig. 7).

We have shown that a simple neural network classifier can improve the detection fidelities over traditional thresholding methods. The neural network classifier does not require assumptions about the system and can incorporate different data sources in one framework in a straightforward way. As the ion-trap systems are very clean and the measurements are well-described theoretically, we do not expect neural networks to beat complicated

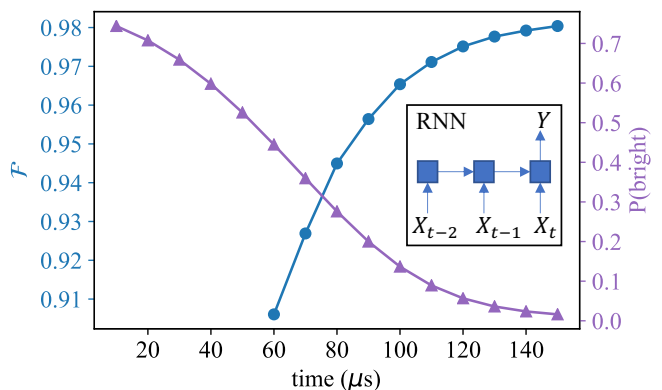


FIG. 7. Recurrent neural network approach. The inset shows a schematic representation of the network, where the carried internal state and the output is affected by additional sequential inputs (time-binned photon counts). Left ordinate, blue circles: Performance of a recurrent network for different detection times. The fidelity increases with longer detection times. Right ordinate, purple triangles: The average probability of the ion being bright decreases with the arrival time of the first photon.

models that take into account possible errors and evaluate the likelihood of a state corresponding to measured values. Similarly, we were not able to observe significant improvements over feed-forward networks by using RNNs or convolutional neural networks. This is because the patterns and correlations in the data are simple and hence well-captured by feed-forward networks. However, we expect our methods to be especially useful in other systems such as superconducting qubits where the measurement processes are more complicated and the data has intricate features.

In addition, we have considered exclusive labels in our classifier, which implies the size of the network scales exponentially with the number of qubits. However, we have observed that multi-label classifiers can achieve a performance close to our method, while maintaining a linear scaling with the number of qubits. Moreover, while it is not necessary in the current setup, by taking advantage of the locality of the crosstalk one can bootstrap smaller networks over a few qubits. By taking majority vote over the outcome of the smaller classifiers, the most probable state corresponding to the measurement results over many qubits is decided.

In conclusion, we expect that techniques such as

the one presented can simplify and improve the future experiments and serve as a straightforward alternative for optimizing the readout of quantum computers as they are scaled up to many qubits.

## ACKNOWLEDGMENTS

AS thanks Evert van Nieuwenburg for helpful discussions. This work was supported by the IARPA LogiQ program, the ARO Atomic Physics program, the ARO and AFOSR MURI programs, Northrup Grumman, and the NSF Physics Frontier Center at JQI.

- 
- [1] P. W. Shor, Phys. Rev. A **52**, R2493 (1995).
  - [2] A. Steane, Proc. R. Soc. Lond. A **452**, 2551 (1996).
  - [3] D. Gottesman, arXiv preprint arXiv:0904.2557 (2009).
  - [4] A. Myerson, D. Szwer, S. Webster, D. Allcock, M. Curtis, G. Imreh, J. Sherman, D. Stacey, A. Steane, and D. Lucas, Physical Review Letters **100**, 200502 (2008).
  - [5] E. Jeffrey, D. Sank, J. Mutus, T. White, J. Kelly, R. Barends, Y. Chen, Z. Chen, B. Chiaro, A. Dunsworth, *et al.*, Physical review letters **112**, 190504 (2014).
  - [6] S. Olmschenk, K. Younge, D. Moehring, D. Matsukevich, P. Maunz, and C. Monroe, Physical Review A **76**, 052314 (2007).
  - [7] A. H. Burrell, *High fidelity readout of trapped ion qubits*, Ph.D. thesis (2010).
  - [8] M. I. Jordan and T. M. Mitchell, Science **349**, 255 (2015).
  - [9] M. A. Nielsen, “Neural networks and deep learning,” (2015).
  - [10] G. Carleo and M. Troyer, Science **355**, 602 (2017).
  - [11] H. Saito, Journal of the Physical Society of Japan **86**, 093001 (2017).
  - [12] X. Gao and L.-M. Duan, Nature communications **8**, 662 (2017).
  - [13] D.-L. Deng, X. Li, and S. D. Sarma, Physical Review X **7**, 021021 (2017).
  - [14] D.-L. Deng, X. Li, and S. Das Sarma, Phys. Rev. B **96**, 195145 (2017).
  - [15] G. Torlai, G. Mazzola, J. Carrasquilla, M. Troyer, R. Melko, and G. Carleo, Nature Physics, 1 (2018).
  - [16] G. Torlai and R. G. Melko, (2018), arXiv:1801.09684.
  - [17] P. Baireuther, T. E. O’Brien, B. Tarasinski, and C. W. Beenakker, Quantum **2**, 48 (2018).
  - [18] S. Krastanov and L. Jiang, Scientific reports **7**, 11003 (2017).
  - [19] G. Torlai and R. G. Melko, Physical Review Letters **119**, 030501 (2017).
  - [20] E. P. van Nieuwenburg, Y.-H. Liu, and S. D. Huber, Nature Physics **13**, 435 (2017).
  - [21] E. van Nieuwenburg, E. Bairey, and G. Refael, arXiv preprint arXiv:1712.00450 (2017).
  - [22] J. Carrasquilla and R. G. Melko, Nature Physics **13**, 431 (2017).
  - [23] S. J. Wetzel, arXiv preprint arXiv:1703.02435 (2017).
  - [24] E. Magesan, J. M. Gambetta, A. Córcoles, and J. M. Chow, Physical review letters **114**, 200501 (2015).
  - [25] S. Debnath, N. M. Linke, C. Figgatt, K. A. Landsman, K. Wright, and C. Monroe, Nature **536**, 63 (2016).
  - [26] M. Acton, K.-A. Brickman, P. Haljan, P. Lee, L. Deslauriers, and C. Monroe, Quantum Information & Computation **6**, 465 (2006).
  - [27] S. G. Crain, *Integrated System Technologies for Modular Trapped Ion Quantum Information Processing*, Ph.D. thesis (2016).
  - [28] C. Shen and L. Duan, New Journal of Physics **14**, 053053 (2012).
  - [29] Y. LeCun, Y. Bengio, and G. Hinton, nature **521**, 436 (2015).
  - [30] M. D. Zeiler, arXiv preprint arXiv:1212.5701 (2012).
  - [31] F. A. Gers, N. N. Schraudolph, and J. Schmidhuber, Journal of machine learning research **3**, 115 (2002).